J. Chem. Sci. Vol. 124, No. 1, January 2012, pp. 51–58.

A quantum-classical simulation of a multi-surface multi-mode nuclear dynamics on $C_6H_6^+$ incorporating degeneracy among electronic states[#]

SUBHANKAR SARDAR and SATRAJIT ADHIKARI*

Department of Physical Chemistry, Indian Association for the Cultivation of Science, Jadavpur, Kolkata 700 032, India
e-mail: pcsa@iacs.res.in

Abstract. We have performed a nuclear dynamics simulation to calculate photoelectron spectra and population profiles of benzene radical cation ($C_6H_6^+$) employing the *parallelized* Time Dependent Discrete Variable Representation (TDDVR) approach. For this purpose, we have considered *two* multi-state multi-mode model Hamiltonians of $C_6H_6^+$ with degeneracy among the electronic states: (a) One consists of three states and eight modes, which in turn leads to a *five state thirteen mode Hamiltonian* (X^2E_{1g}-B^2E_{2g}-C^2A_{2u}) due to the degeneracy; and (b) The other is constituted of three states and thirteen modes which is basically a *five state twenty mode Hamiltonian* (B^2E_{2g}-D^2E_{1u}-E^2B_{2u}) for the same reason. Since these electronic states are interconnected by several conical intersections in the vicinity of the Franck Condon region, it will be *challenging* to pursue such large dynamical calculation in the presence of nonadiabaticity among the electronic states. The spectral as well as population profiles calculated with the advent of TDDVR approach show reasonably good agreement with the results obtained by the Multi Configuration Time Dependent Hartree (MCTDH) methodology.

Keywords. Multi surface multi mode quantum dynamics; parallelized quantum classical approach; TDDVR method.

1. Introduction

Calculations of dynamical phenomena originating from nonadiabatic processes,[1–7] particularly, in the presence of conical intersections (CIs) require a rigorous quantum mechanical (QM) treatment[8] whereas traditional QM approaches are impractical even for three or four particle systems as computational time increases exponentially with the degrees of freedom (DOFs). The quantum correction to classical mechanics is one of the avenues to develop a first principle based quantum-classical theory to achieve the following purposes: (i) the method can distinguish dynamical regimes of a system like quasi-classical and deep quantum; (ii) it can treat the deep quantum regime rigorously and quasi-classical regime classically with some mild quantum corrections. One successful way to meet these two requirements is the use of a Gaussian wave packet (GWP)[9] and its' extension, the Gauss-Hermite (GH) basis set.[10–12]

The TDDVR method[13–16] is formulated by using the GH basis function as the primitive one and such basis with DVR representation makes the method efficient than the other contemporary approaches with the following distinct advantages: (a) a small number of optimized set of asymmetrically dense grid points are generated from the Hermite polynomial associated with the eigenfunction of a harmonic oscillator defined around the centre of an initial wave packet, GWP; (b) the "classical" dynamics of the time dependent parameters of a GWP dictates the movement of these unevenly spaced grid points; (c) though the evaluation of kinetic energy (KE) matrices is needed once for the entire propagation, the diagonal potential energy matrix by which the electronic states are coupled has to be calculated at each time step; (d) the contributions of different modes on the time derivative of an amplitude can be calculated independently and thereby, motivate us to *parallelize the algorithm*.

The TDDVR approach is a well established molecular dynamics simulation method for relatively large molecular systems.[17–20] At present, we have implemented the method for two multi-mode multi-surface model Hamiltonians of $C_6H_6^+$ to explore its' workability with respect to other contemporary methodologies,[21,22] where the formulation consists of the following

[#]Dedicated to Prof. N Sathyamurthy on his 60th birthday
*For correspondence

assumptions on the form of the molecular wavefunction: (a) the total wavefunction is expressed as a linear combination of the product type TDDVR basis functions of different modes with time dependent coefficients; (b) the TDDVR basis set is obtained by multiplying the DVR basis with a plane wave; (c) the DVR basis functions are constructed by using the eigenfunctions of harmonic oscillator as the primitive one; (d) the plane wave is defined by a 'classical' trajectory and its' momentum. When this multi-dimensional multi-surface wavefunction matrix is substituted in the TDSE, the time dependence of the expansion coefficients brings the quantum dynamics and the 'classical' equation of motion for the central trajectory with its' momentum appears naturally. Since the width parameter appears with the off- and on-diagonal elements of the TDDVR quantum equation of motion, we choose the parameter time independent to bypass inaccuracy arising through the stiffness of the corresponding 'classical' equation of motion. This formulation has the scope to derive the variationally optimized 'classical' equation of motion from first principles leading to quantum corrections in the 'classical' trajectory or 'classical' feedback to the quantum dynamics in a self consistent manner. In our previous articles,[16,17] different computational aspects of TDDVR method and other contemporary time dependent techniques, namely fast Fourier transformation[23] method, nested interaction representation[24] method, distributed approximating function[25] approach and other time dependent DVR method[26] were described elaborately in a comparative manner.

Benzene is a prototype organic radical cation consisting five lowest electronic states,[27] X^2E_{1g}, B^2E_{2g}, C^2A_{2u}, D^2E_{1u} and E^2B_{2u}, which in view of degeneracy present in X^2E_{1g}, B^2E_{2g} and D^2E_{1u} states generate eight potential energy surfaces.[28,29] Even though many theoreticians investigated[27–32] the $C_6H_6^+$ system, the first quantum-dynamics study incorporating degeneracy among the electronic surfaces was carried out by Köppel *et al.*[29] Such multi-dimensional dynamical simulation on molecular system is a great challenge for theoreticians. Since we have already carried out the dynamics on $C_6H_6^+$ including five non-degenerate surfaces,[18] it will be interesting to explore the nuclear dynamics of the same cation, where the Hamiltonian[28,29] is constituted with strongly vibronically coupled doubly degenerate electronic states as well as DOFs. A preliminary investigation on the Hamiltonian was carried out in one[20] of our recent articles, where *less* computational effort was needed than this present work.

2. The model and theoretical background of TDDVR approach

2.1 *The Hamiltonian*

Since we have previously considered[18,19] the five surfaces of $C_6H_6^+$ excluding degeneracy in X^2E_{1g}, B^2E_{2g} and D^2E_{1u} states, the aim of our present dynamical calculation is to explore the workability of *parallelized* TDDVR approach on two degenerate model Hamiltonians of $C_6H_6^+$: (a) one includes *five-state and thirteen-modes* (X^2E_{1g}-B^2E_{2g}-C^2A_{2u}); (b) the other comprises of *five states and twenty modes* (B^2E_{2g}-D^2E_{1u}-E^2B_{2u}). For present dynamical calculation, we adopt two suitable model Hamiltonians,[28,29] with corresponding coupling parameters and ionization potential values of $C_6H_6^+$.

2.2 *The time-dependent discrete variable representation method*

The detailed formulations of the different versions of TDDVR approach have been presented elsewhere,[14–17] therefore, we briefly demonstrate the relevant equations used for current perspective in the simplest way. The scheme propagates the DVR grid-points by utilizing the 'classical' equation of motion with a time-independent width parameter in the primitive basis set. Considering the Hamiltonians for $C_6H_6^+$, the TDSE in the diabatic representation is given by:

$$i\hbar\frac{\partial}{\partial t}\Xi(\{Q_k\},t) = \left[\hat{\mathbf{T}}_{\{Q_k\}} + \hat{\mathbf{V}}(\{Q_k\})\right]\Xi(\{Q_k\},t), \quad (1)$$

where

$$\Xi(\{Q_k\},t) \equiv \begin{pmatrix} \Psi_1(\{Q_k\},t) \\ \Psi_2(\{Q_k\},t) \\ \cdots \\ \Psi_l(\{Q_k\},t), \end{pmatrix}, l = 1, 2, ..., 5 \quad (2)$$

with $\int \Xi^{\dagger}(\{Q_k\},t)\Xi(\{Q_k\},t)\prod_{k=1}^{p} dQ_k = 1$ at any time t. The lth diabatic wavefunction $[\Psi_l(\{Q_k\},t)]$ for many DOF (p) is expanded in terms of products of TDDVR basis functions $[\{\psi_{i_k}(Q_k,t)\}]$ for the different (k) modes,

$$\Psi_l(\{Q_k\},t) = \sum_{i_1 i_2 \ldots i_p} c_{i_1 i_2 \ldots i_p, l}(t)\prod_{k=1}^{p}\psi_{i_k}(Q_k,t), \quad (3)$$

and the i_kth basis for the kth mode is again expressed with DVR basis multiplied by plane wave to represent the coordinate, Q_k, as a function of time, t,

$$\begin{aligned}\psi_{i_k}(Q_k,t) &= \phi(Q_k,t)\sum_{n=0}^{N_k}\xi_n^*(x_{i_k})\xi_n(x_k)\\ &= \sum_{n=0}^{N_k}\xi_n^*(x_{i_k})\Phi_n(Q_k,t),\\ \phi(Q_k,t) &= \pi^{1/4}e^{\frac{i}{\hbar}\{P_{Q_k^c}(t)[Q_k-Q_k^c(t)]\}},\end{aligned} \tag{4}$$

where harmonic oscillator eigenfunctions are the primitive basis to construct DVR functions,

$$\begin{aligned}\xi_n(x_k) &= \left(\frac{2ImA_k}{\pi\hbar}\right)^{1/4}\frac{e^{-\frac{x_k^2}{2}}}{\sqrt{n!2^n\sqrt{\pi}}}H_n(x_k),\\ x_{i_k} &= \sqrt{\frac{2ImA_k}{\hbar}}(Q_{i_k}(t)-Q_k^c(t)).\end{aligned} \tag{5}$$

A TDDVR grid-point, Q_{i_k}, is determined by (5) using the root, x_{i_k}, of N_kth Hermite polynomial, $H_{N_k}(x_k)$. Although the roots (x_{i_k}s) of the polynomial are fixed values but the positions of the TDDVR grid-points (Q_{i_k}s) will change as a function of time due to the time-dependent variables, $Q_k^c(t)$. When the model Hamiltonians[29] and the TDDVR representation of wavefunction (2)–(5) are substituted into the TDSE (1), the classical path picture appears naturally along with the quantum equation of motion. The expression of the differential equation for an amplitude, $d_{i_1i_2....i_p,l}$ on the lth surface is,

$$\begin{aligned}i\hbar\dot{d}_{i_1i_2...i_p,l} &= \frac{1}{2}\left\{\sum_k \dot{P}_{Q_k^c}\sqrt{\frac{\hbar}{ImA_k}}\,\bar{G}_{i_ki_k}\right\}d_{i_1i_2...i_p,l}\\ &+ \left\{\sum_k\frac{\mu(\dot{Q}_k^c)^2}{2}\right\}d_{i_1i_2...i_p,l}\\ &+ \sum_k\left\{\frac{\hbar ImA_k}{2\mu}\sum_{i_1'i_2'...i_p'}\bar{F}_{i_ki_k'}\right.\\ &\times \left.d_{i_1'i_2'...i_p',l}\prod_{k'\neq k}^{p}\delta_{i_{k'}i_{k'}'}\right\}\\ &+ V_{ll}\left(i_1i_2...i_p\right)d_{i_1i_2...i_p,l}\\ &+ \sum_{l'\neq l}V_{ll'}\left(i_1i_2...i_p\right)d_{i_1i_2...i_p,l'}.\end{aligned} \tag{6}$$

The explicit expression of the component matrices of the TDDVR equations of motion[14–17] and their properties are presented in *supplementary material*. Moreover, the classical path equations for the kth mode, those appear along with the quantum equation of motion, can be written as

$$\dot{Q}_k^c(t) = \frac{P_{Q_k^c}(t)}{\mu}, \tag{7}$$

$$\dot{P}_{Q_k^c}(t) = -\frac{dV(\{Q_k\})}{dQ_k}\Big|_{Q_k(t)=Q_k^c(t)} + Q_k^F(t), \tag{8}$$

where $Q_k^F(t)$ is the quantum force for the kth mode whose rigorous expression[15–17] is presented in *supplementary material*. The dynamical evolution of the system is being performed by simultaneously solving the set of differential equations (6), (7) and (8).

3. The numerical details and photoelectron spectra

The optimum numbers of TDDVR grid-points used to perform the dynamics on $C_6H_6^+$ are presented in table 1. The dynamics is carried out with many TDDVR basis functions for important vibrational modes but with very few number of basis functions for the less important and unimportant modes. We describe the coupling and tuning modes with sufficient number of TDDVR basis to reach the quantum limit, where the centroid of the wave packet of such modes obey the Ehrenfest theorem. In the classical limit, some of the coupling modes are accounted only with one TDDVR basis function and the propagation of the lone grid-point is dictated only by classical dynamics in the Newtonian sense. In

Table 1. The optimum number of TDDVR basis functions used in dynamical calculation of $C_6H_6^+$.

System	Normal modes	Basis functions	Total basis sets
X-B-C	ν_1, ν_2, ν_{16x}, ν_{17x}, ν_{18x}, ν_{19x}, ν_{20x}, ν_{16y}, ν_{17y}, ν_{18y}, ν_{19y}, ν_{20y}, ν_{eff}	2, 11, 9, 1, 9, 7, 1, 9, 2, 2, 9, 2, 3	121247280
B-D-E	ν_1, ν_2, ν_5, ν_6, ν_9, ν_{10}, ν_{12x}, ν_{13x}, ν_{14x}, ν_{15x}, ν_{16x}, ν_{17x}, ν_{18x}, ν_{12y}, ν_{13y}, ν_{14y}, ν_{15y}, ν_{16y}, ν_{17y}, ν_{18y}	2, 13, 2, 9, 1, 2, 1, 1, 1, 1, 7, 5, 5, 1, 1, 1, 1, 7, 5, 5	143325000

the TDDVR formulation with sufficient number of grid-points, the calculated results appear as independent of the initial choice of 'classical' momentum of the central trajectory and thereby, we have chosen $Q_i(t_0) = 0$ and $P_i(t_0) = 0$ for those modes. On the other hand, this choice plays a key role when a mode is treated with single grid-point because then the dynamics is solely dictated by classical mechanics. In this calculations, the choice of classical parameters for one grid-point dynamics are $Q_i(t_0) = 0$ and $P_i(t_0) = \sqrt{\hbar m \omega_i}$. It is worthwhile to mention that the present TDDVR algorithm solves more than 14×10^7 number differential equations *simultaneously* at each time step and such computational effort is much demanding than all our previous studies.[16–20]

The prime interest of this article is to theoretically calculate the photoelectron spectrum of $C_6H_6^+$. The TDDVR method is used to propagate the nuclear wavefunction and thereby, to calculate the autocorrelation function $[C(t)]$ where the Fourier transform of $C(t)$ gives photoelectron spectra of $C_6H_6^+$:

$$I(\omega) \propto \omega \int_{-\infty}^{\infty} C(t) \exp(i\omega t) dt, \tag{9}$$

where

$$C(t) = \langle \Psi(t) | \Psi(0) \rangle \tag{10}$$

$$= \left\langle \Psi^*\left(\frac{t}{2}\right) \middle| \Psi\left(\frac{t}{2}\right) \right\rangle. \tag{11}$$

(11) is more accurate, computationally faster and convenient to implement than equation (10). On the other hand, (11) is valid only if the initial wavefunction is real and the Hamiltonian is symmetric. In the time-dependent picture, the phenomenological broadening of the spectra is equivalent to damping the autocorrelation function by a time-dependent function as chosen below:

$$h(t) = \exp\left[-\left(\frac{|t|}{\tau}\right)^2 \right] \tag{12}$$

with an appropriate parameter, τ. we perform numerical calculations starting with an initial wave packet $\Psi(0)$ from the C^2A_{2u}/E^2B_{2u} electronic state. The numerical propagation of $\Psi(t)$ is then performed to obtain the corresponding spectra according to (9).

4. Results and discussion

4.1 *Calculation of spectra*

In our previous calculation,[18] we have evaluated the B^2E_{2g} - C^2A_{2u} band of $C_6H_6^+$ considering nondegenerate Hamiltonian[27] and in this segment, we present the same spectra considering degeneracy among those states. The X-B-C Hamiltonian[29] comprises of three electronic surfaces and eight vibrational modes, namely ν_1, ν_2, ν_{eff} and ν_{16} - ν_{20}, which in view of doubly degeneracy of the X^2E_{1g} and B^2E_{2g} state shows thirteen DOFs with five electronic states. These vibrational modes can be classified as: ν_1 + ν_2 the totally symmetric modes, whereas ν_{16} - ν_{18} and ν_{19} - ν_{20} behave as Jahn-Teller (JT) and pseudo JT (PJT) coupling modes, respectively. Since the contribution of the JT mode ν_{18} is substantial in this spectra, it demands a greater number of TDDVR basis functions (see table 1). We have carried out our dynamical calculations separately locating the initial wave packet at $Q = 0$ on B as well as C state and obtained the corresponding individual bands as displayed in figure 1(a) and (b), respectively. Sum of these TDDVR calculated individual spectrum leads to the B - C band, which is presented in figure 2(a) along with the MCTDH calculated[29] (figure 2(b)) and experimental[33] (figure 2(c)) ones. It is important to note that the individual and total spectra are calculated with different damping parameter for best fit with the MCTDH as well as experimental profiles and thereby, the overall agreement among these spectra are quite satisfactory.

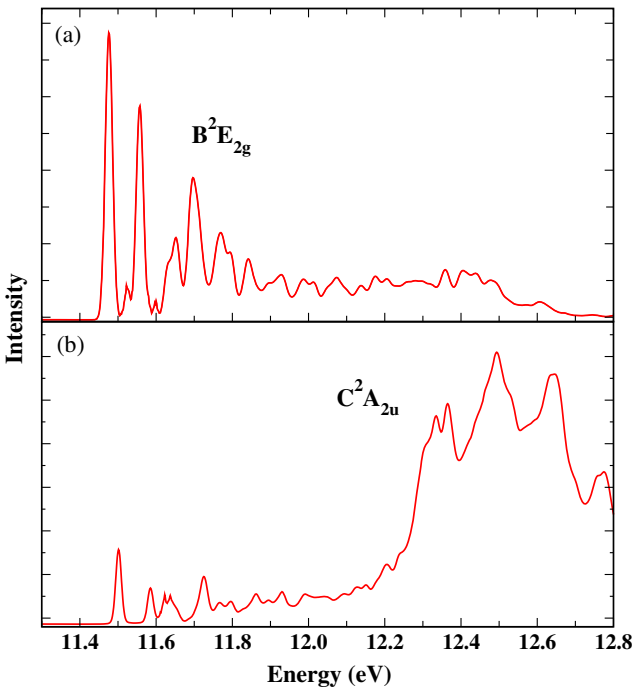

Figure 1. (**a**) and (**b**) present the TDDVR calculated spectral profiles for B^2E_{2g} and C^2A_{2u} bands, respectively, which are calculated with damping parameter, $\tau = 9.7 \times 10^{-14}$ s. Both the spectra are scaled to same height for clear visualization.

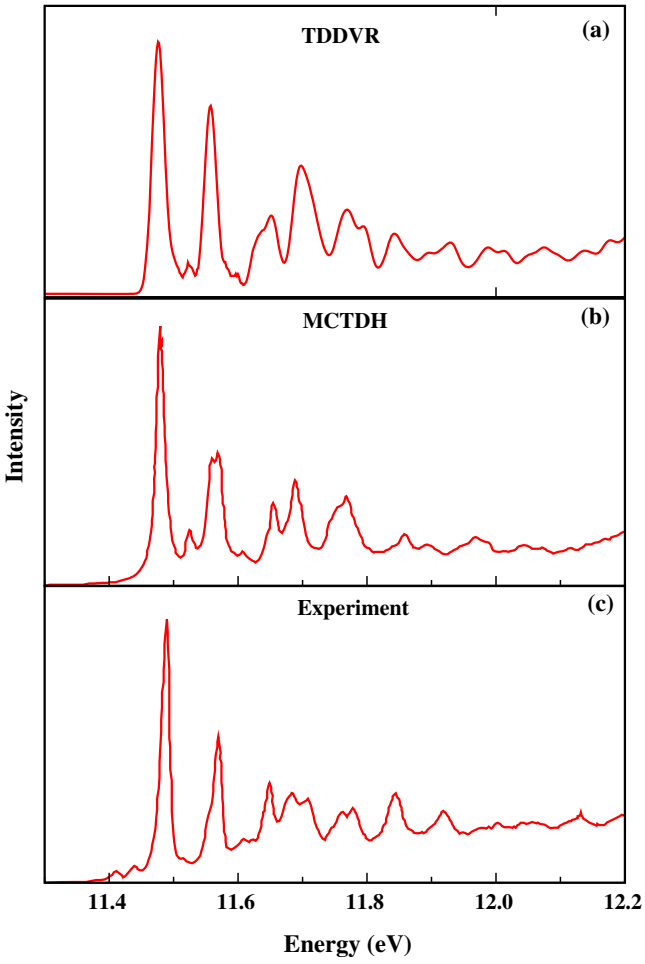

Figure 2. (**a**), (**b**) and (**c**) present the B^2E_{2g} - C^2A_{2u} band obtained by TDDVR approach, MCTDH method and experiment technique, respectively, where TDDVR calculated spectra are calculated with $\tau = 3.5 \times 10^{-14}$s.

Similarly, the individual D^2E_{1u} and E^2B_{2u} bands are also calculated by performing the dynamics on the *B-D-E* Hamiltonian[29] locating the initial wavepacket on the corresponding states and the spectral profiles are displayed in figure 3. In order to compute the spectra, we account opposite relative signs of the JT coupling constants[29] in case of *B* and *D* states. The thirteen vibrational modes (ν_1, ν_2, ν_5, ν_6, ν_9, ν_{10} and ν_{12} - ν_{18}) of the *B-D-E* Hamiltonian become *twenty DOFs* due to degeneracy. Among the *twenty* vibrational modes, we have treated eleven DOFs quantum mechanically leading to almost $\sim 15 \times 10^7$ number of TDDVR basis sets (see table 1). The TDDVR calculated results for B^2E_{2g} - C^2A_{2u}, D^2E_{1u} and E^2B_{2u} bands are obtained by considering degenerate states in the Hamiltonians and show reasonable agreement with the MCTDH calculated[29] spectra.

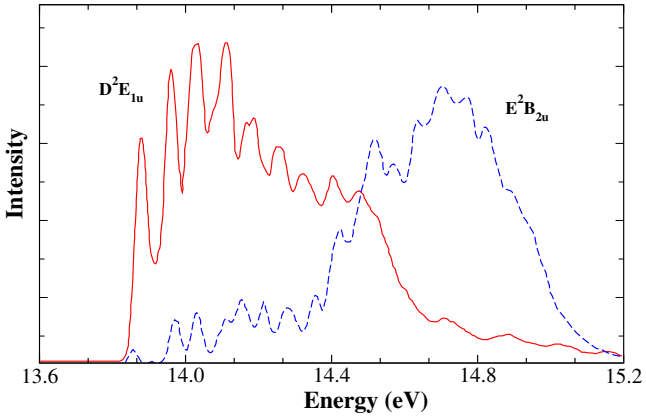

Figure 3. (**a**) and (**b**) present the TDDVR calculated spectral profiles for D^2E_{1u} and E^2B_{2u} state, respectively, which are calculated with $\tau = 4.5 \times 10^{-14}$ s.

4.2 *Population dynamics*

In this segment, we discuss dynamical properties of X^2E_{1g} - B^2E_{2g} - C^2A_{2u} and B^2E_{2g} - D^2E_{1u} - E^2B_{2u} systems of the $C_6H_6^+$ comprises of two five-surface Hamiltonians,[29] where the calculations are performed locating the initial wave packet on the uppermost state (C^2A_{2u} or E^2B_{2u}) of both systems at the FC point, $Q = 0$. The diabatic population dynamics on the *X-B-C* system are presented in figure 4(a), where the solid, dashed and dotted lines indicate the profiles for *C*, *B* and *X*

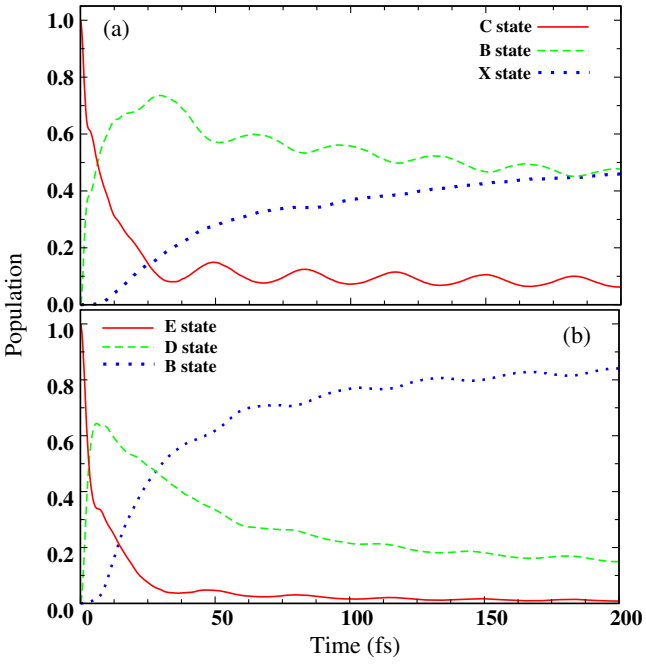

Figure 4. (**a**) and (**b**) display the population profiles of *X-B-C* and *B-D-E* system when time-dependent dynamics is performed locating the initial wavepacket at FC point of C^2A_{2u} and E^2B_{2u} surface, respectively.

state, respectively. The important features of these profiles are: (i) the population of C state rapidly decays to reach almost zero (within 50 fs) and then, it shows a slight oscillations around low (10%) population range; (ii) on the contrary, B state population sharply increases to attain almost 70% before it decays slowly with mild oscillations; (iii) unlike B and C state, the X state shows a slow increment of population till the dynamics ends. On the other hand, the population profiles for B-D-E system are presented in panel (b) of figure 4, where the solid, dashed and dotted lines indicate the E, D and B state, respectively. These profiles have similarity and differences with X-B-C system as: (i) The upper E state population (solid) decays very fast similar to C state in X-B-C but the oscillations are absent; (ii) The lowest B state (dotted) shows fast increment of population up to $\sim$ 82%, which is, indeed, much greater than the maximum value of the X state population in X-B-C system. The population profiles of both the systems calculated by TDDVR method show a good agreement with the MCTDH calculated profiles.[29]

5. Summary: Computational advantages of parallelized TDDVR approach

Since a series of CIs lies among the various electronic states of $C_6H_6^+$, the multi-state multi-mode model Hamiltonians naturally involve a complex dynamics and develop a rich structure in the photoelectron spectra through the vibronic coupling mechanism. Such system with many electronic states and vibrational DOFs provide a scope to explore the workability of our *parallelized* TDDVR approach. We perform the molecular dynamics by employing the *parallelized* version of TDDVR algorithm considering *two* multi-surface multi-mode Hamiltonians to calculate its' various dynamical properties, namely photoelectron spectra and population dynamics due to the electronic excitation.

The aim of our present article is to formulate an accurate and efficient numerical algorithm that can (i) accommodate many vibrational modes and electronic surfaces, (ii) reproduce the experimental and other theoretically calculated spectra and population/nuclear dynamics, (iii) perform the calculation within a reasonable real time scale. Since we have already demonstrated the workability of the TDDVR methodology in terms of accuracy of the calculated spectra and population dynamics in the *Results and discussion* section, the following paragraphs are devoted only to present the efficiency of the algorithm.

Though the number of DOFs involved in quantum dynamics is restricted by exponentially increasing computation time, it becomes possible to increase the dimension of our numerical problems considerably with the advent of massive parallel computers, where thousands of processors may work on a single task. In parallel computing, the large problems may be divided into smaller ones algorithmically and then, could be solved concurrently ('in parallel') with less elapsed time. Our TDDVR algorithm is implemented in such a way that it can handle large quantum systems within reasonable wall clock time. While implementing the programme, we choose carefully the loops to parallelize, i.e., for an efficient parallelization, it is very important to identify the most time consuming parts of the code. The TDDVR algorithm has a clear scope to scale down the necessity of CPU time, because it has the natural possibility[17,19] to parallelize the major areas of its' algorithm. The evaluation of the time derivative amplitude vector ($\dot{d}_{i_1 i_2 \ldots i_p, l}$) in TDDVR equation of motion [the third term in the r.h.s. of (6)] consumes almost 94% of total computation time, whereas the rest of the time is spent to calculate time-dependent wave function vector ($d_{i'_1 i'_2 \ldots i'_p, l}$).

It is often possible to reduce the execution time of the large dimensional systems by TDDVR algorithm by exploiting *loop-level parallelism*, i.e., by executing iterations of the loops concurrently across multiple processors. Therefore, we can reduce our computational effort by employing both the shared-memory (SM) as well as distributed-memory (DM) parallelization scheme. In order to obtain the numerical

Table 2. A comparison between the computation time of serial and parallelized TDDVR algorithm to study molecular dynamics of $C_6H_6^+$.

System	No. of processors	Computation time (in hr.)	Speedup (S_p)
	1	106.5	-
	2	88.5	1.2
	4	29.5	3.6
X-B-C	8	15.6	6.8
	16	7.5	14.0
	32	4.1	26.0
	60	6.8	15.6
	1	83.0	-
	2	75.4	1.1
	4	23.0	3.6
B-D-E	8	12.0	6.9
	16	5.6	14.7
	32	3.1	26.7
	60	4.3	19.3

magnitude of the (6) at each time step, we need to evaluate the product [the third term in the r.h.s. of (6)], which comprises the multiplication between wavefunction vector ($d_{i'_1 i'_2 \ldots i'_p, l}$) and KE matrix, $\bar{F}_{i_k i'_k}$. Interestingly, the contributions of different modes on a time-dependent amplitude ($\dot{d}_{i_1 i_2 \ldots i_p, l}$) can be evaluated independently. Since the evaluation of this matrix-vector product consumes maximum CPU time and such product for a particular mode of a surface is *totally independent* (sparse matrix-vector multiplication) from other modes and surfaces, these calculations are parallelized on a multiple core cluster with shared memory using OpenMP based architecture on the single process (function) - multiple data (*spmd*) parallelization scheme.

Our implementation depends upon SM parallelization, because in this parallelization, no communication among master and slave nodes is required and it is more efficient than DM parallelization. The latter may be implemented on master-slave parallelization scheme using MPI and that would entail master slave communication overhead.

In this numerical investigation, we present the advantage of the parallelized TDDVR algorithm over its' serial analog, where the dynamics has been carried out by using $\sim 3 \times 10^7$ number of TDDVR basis functions on each surface (see table 1) involving five-state model Hamiltonian[29] for $C_6H_6^+$. We have carried out all the calculations on a IBM - P - 590 cluster equipped with 32 Dual - Core (two CPUs in each LPAR) computing nodes (LPARs) with a single symmetric multiprocessing (SMP) configurations. The amount of elapsed time needed to perform the dynamical simulation for $C_6H_6^+$ are shown in table 2, which demonstrates *various* speedup due to parallelization of the programme.

The speedup, S_p, which is a measure of the gain of using multiple processors with respect to the single one, is, therefore, defined as $S_p = T_1/T_p$, where p denotes the number of processors, T_p and T_1 indicate the execution time of the parallel algorithm with p processors and sequential algorithm, respectively. Table 2 demonstrates that with increasing number of processors, the elapsed time rapidly reduces at first and then, remains almost same or even increases due to the sharing and synchronization overhead. Since the product between the number of actively participating vibrational modes and electronic states involved in our dynamical calculation for both the systems (*X-B-C* and *B-D-E*) is around thirty five (35), the required number of processors to parallelize those equations of motion is expected to be of the same order. If we include more processors than the required number ($\sim$ 32), obviously the overhead for parallelization increases ($\sim$ 60) as shown in table 2. In summary, *our parallelized TDDVR algorithm reduces the computation time more than an order of magnitude compare to its serial analog.*

Supplementary information

The electronic supporting information can be seen in http://www.ias.ac.in/chemsci.

Acknowledgements

SS acknowledges the Council of Scientific and Industrial Research (CSIR), India, for a research fellowship and SA acknowledges the Department of Science and Technology (DST Government of India) for financial support through the project no. SR/S1/PC - 13/2008 - 2011.

References

1. Herzberg G and Longuet-Higgins H C 1963 *Discuss. Faraday Soc.* **35** 77
2. Yarkony D R 1996 *Rev. Mod. Phys.* **68** 985
3. Köppel H, Domcke W and Cederbaum L S 1984 *Adv. Chem. Phys.* **57** 59
4. Baer M and Englman R 1997 *Chem. Phys. Lett.* **265** 105
5. Baer M 1997 *J. Chem. Phys.* **107** 10662
6. Baer M 2006 in *Beyond Born-Oppenheimer: Electronic Nonadiabatic Coupling Terms and Conical Intersections* (Hoboken: Wiley-Interscience)
7. Adhikari S and Billing G D 2002 *Adv. Chem. Phys.* **124** 143
8. Schatz G and Ratner M A 1993 *Quantum mechanics in chemistry* (Englewood Cliffs, NJ: Prentice Hall)
9. Heller E J 1975 *J. Chem. Phys.* **62** 1544
10. Lee S Y 1986 *Chem. Phys.* **108** 451
11. Lee S Y and Heller E J 1982 *J. Chem. Phys.* **76** 3035
12. Meyer H -D 1981 *Chem. Phys.* **61** 365
13. Adhikari S and Billing G D 2000 *J. Chem. Phys.* **113** 1409
14. Barkakaty B and Adhikari S 2003 *J. Chem. Phys.* **118** 5302
15. Puzari P and Adhikari S 2004 *Int. J. Quant. Chem.* **98** 434
16. Puzari P, Sarkar B and Adhikari S 2005 *Int. J. Quant. Chem.* **105** 209
17. Puzari P, Swathi R S, Sarkar B and Adhikari S 2005 *J. Chem. Phys.* **123** 134317
18. Sardar S, Paul A K, Sharma R and Adhikari S 2009 *J. Chem. Phys.* **130** 144302
19. Sardar S, Paul A K, Sharma R and Adhikari S 2011 *Int. J. Quant. Chem.* **111** 2741
20. Sardar S, Paul A K and Adhikari S 2010 *J. Chem. Sc.* **122** 491
21. Meyer H -D, Manthe U and Cederbaum L S 1990 *Chem. Phys. Lett.* **165** 73

22. Meyer H -D, Gatti F and Worth G A 2009 *Multidimensional quantum dynamics: MCTDH theory and applications* (Weinheim: WILEY-VCH Verlag GmbH & Co. KGaA)
23. Kottler Z, Nitzan A and Kosloff R 1988 *Chem. Phys. Lett.* **153** 483
24. Tannor D J, Besprozvannaya A and Williams C J 1992 *J. Chem. Phys.* **96** 2998
25. Kouri D J, Ma X, Zhu W, Petit B M and Hoffman D K 1992 *J. Phys. Chem.* **96** 9622
26. Sim E and Makri N 1995 *J. Chem. Phys.* **102** 5616
27. Baldea I and Köppel H 2006 *J. Chem. Phys.* **124** 064101
28. Döscher M, Köppel H and Szalay P G 2002 *J. Chem. Phys.* **117** 2645
29. Köppel H, Döscher M, Baldea I and Meyer H -D 2002 *J. Chem. Phys.* **117** 2657
30. Köppel H, Cederbaum L S and Domcke W 1988 *J. Chem. Phys.* **89** 2023
31. Köppel 1993 *Chem. Phys. Lett.* **205** 361
32. Döscher M and Köppel H 1997 *Chem. Phys.* **225** 93
33. Balzer P, Karlsson L, Wannberg B, Öhrwall G, Holland D M P, MacDonald M A, Hayes M A and Niessen W von 1997 *Chem. Phys.* **224** 95